ELSEVIER

Contents lists available at ScienceDirect

# Scripta Materialia

journal homepage: www.journals.elsevier.com/scripta-materialia





# Origin of morphological variation of grain boundary precipitates in titanium alloys

Rongpei Shi a,b,\*, Dian Li c, Stoichko Antonov d, Xingjun Liu a,b, Yufeng Zheng c,\*

- <sup>a</sup> School of Materials Science and Engineering, Harbin Institute of Technology, Shenzhen 518055, China
- b Institute of Materials Genome and Big Data, Harbin Institute of Technology, Shenzhen 518055, China
- <sup>c</sup> Department of Chemical and Materials Engineering, University of Nevada Reno, Reno, NV 89557, USA.
- d Department of Microstructure Physics and Alloy Design, Max-Planck-Institut für Eisenforschung GmbH, 40237 Düsseldorf, Germany.

## ARTICLE INFO

Keywords:
Titanium
Precipitation
3D Characterization
Computer simulation
Phase-field method

#### ABSTRACT

Morphological variations of grain boundary (GB) allotriomorphs and widmanstatten sideplates (WS) of  $\alpha$  precipitate in a  $\beta$  titanium alloy, have been systematically investigated by combining three-dimensional (3D) phase-field simulations, 3D experimental characterization and crystallographic orientation analysis. The inclination angle,  $\theta$ , between the habit plane of the GB $\alpha$  and the hosting GB plane is found to dictate the morphologies of GB precipitates. For the first time, three distinct regimes of  $\alpha$  morphology at a  $\beta$  GB, separated by two critical angles  $(\theta_c^1, \theta_c^2)$  are observed:  $\theta \leq \theta_c^1$ , GB $\alpha$  alone decorates the GB as a continuous layer;  $\theta_c^1 < \theta \leq \theta_c^2$ ,  $\alpha$  precipitate appears as a mixture of GB $\alpha$  and a WS emanating from it;  $\theta > \theta_c^2$ , WS alone grows directly from bare  $\beta$  GBs. The dramatic morphological variation owes its origin to the dynamic interplay between the spreading along GBP and the intragranular growth of the GB precipitate, and its dependence on  $\theta$ .

Titanium alloys predominantly derive their strength from the interfaces between the second-phase  $\alpha$  precipitates and the  $\beta$  matrix that serve as the barrier to dislocation motion [1]. Thus, understanding, prediction and control of the size, morphology and spatial distribution including that of its orientation variants of  $\alpha$  precipitates are highly desirable for engineering desired microstructures for optimal properties targeting specific applications [2,3,4]. Two distinctive types of morphology for  $\alpha$  precipitates at or near prior  $\beta$  grain boundaries (GBs), namely GB allogriomorphs (GB $\alpha$ ) and widmanstatten side-plates (WS) [1,5,6], have been commonly observed during  $\beta$ -processing heat treatment. In general, GB $\alpha$ s first nucleate and grow along the hosting  $\beta$  GBs upon cooling. On the one hand, GB $\alpha$  may appear as a continuous  $\alpha$  layer consisting of a single variant or as a group of discrete near-equiaxed particles consisting of alternating crystallographic variants but physically isolated by  $\beta$  phase. On the other hand, WS may emanate from GB $\alpha$ that has already nucleated at and grown to occupy the  $\beta$  GBs [7]. The resulting WS, however, may either inherit the crystallographic orientation of the  $GB\alpha$  or have a different one [8,9]. Furthermore, discrete WS could grow directly from bare  $\beta$  GBs without forming a GB $\alpha$  [5].

Even though significant variations in the morphology of both  $GB\alpha$  and WS have been frequently reported by independent experimental

studies, it remains inclusive that under what conditions GB $\alpha$  is preferred over WS and vice versa, let alone the resulting morphology [1]. It is generally accepted that the orientation and morphology of  $\alpha$  precipitates at or near  $\beta$  GBs are dictated by the variant(s) selected for the GB $\alpha$  at the specific GB. Variant selection (VS) of GB $\alpha$  is, to a large extent, governed by the structure of the boundary that is macroscopically characterized by misorientation, and inclination of the grain boundary plane (GBP) [10]. Numerous experimental and theoretical studies have been carried out to investigate how the structure of a prior  $\beta$  GB contribute to VS of  $GB\alpha$  and WS [5,10–14], and several empirical rules have been proposed based on experimental observations and some intuitive understanding of the possible mechanisms of the  $\beta$  to  $\alpha$  transformation [1,5,8,13,15,16]. One of such rules (on the effect of GBP inclination) is that the variant selected should have the smallest angle between the low-energy interface of  $GB\alpha$  (i.e., its habit plane (HP)) and the GBP [16]. However, the rule (even when used in conjunction with other VS rules about misorientation) has been found to be frequently violated by independent studies [10], suggesting not only that the underlying mechanisms of VS of  $\alpha$  precipitate at  $\beta$  GB remain inclusive, but also that the HP of the selected GB $\alpha$  may make a random inclination angle (defined as  $\theta$  hereafter) relative to the GBP. Thus, the key hypothesis behind this study is

E-mail addresses: shirongpei@hit.edu.cn (R. Shi), yufengz@unr.edu (Y. Zheng).

<sup>\*</sup> Corresponding author.

Scripta Materialia 214 (2022) 114651

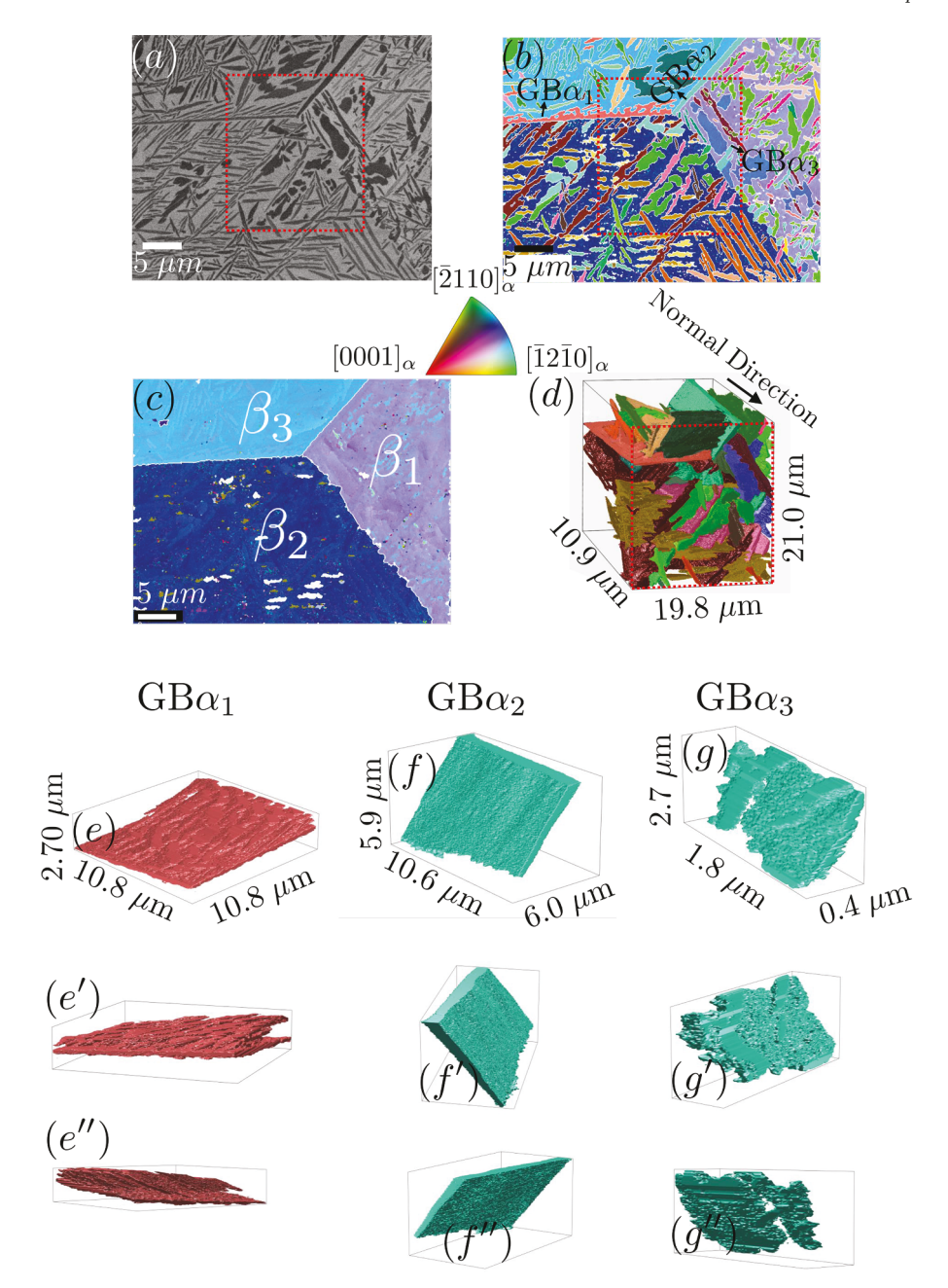


**Fig. 1.** (a) BSE, (b) EBSD OIM images for  $\alpha$  phase precipitate microstructure; (c) Reconstructed  $\beta$ -phase orientation map; (d) 3D images of the  $\alpha$  precipitates formed at and near GBs in the region highlighted by the dashed square in (a); (e)-(f): 3D morphologies of GB $\alpha$ <sub>1</sub>, GB $\alpha$ <sub>2</sub> and GB $\alpha$ <sub>3</sub>, as viewed from different directions.

that the randomness of the inclination angle  $\theta$  may contribute to the morphological variations of  $\alpha$  precipitate at or near  $\beta$  GBs.

Herein, we investigate the effect of  $\theta$  on the morphological development of GB precipitates by integrating three-dimensional (3D) phase field simulations with 3D experimental characterization, combining focused ion beam/scanning electron microscopy (FIB/SEM) topography and crystallographic orientation analysis. The former allows for a comprehensive mapping of the development of GB $\alpha$  and WS and their interplay as a function of  $\theta$  while the latter is essential for an unambiguous analysis of the grain morphologies in 3D space and for designing and validating simulations [17,18,19,20]. It is identified, for the first time, that there exist three distinct regimes in which the morphology of GB precipitates varies from one to another: with increasing  $\theta$  from 0 to 90°, the morphology varies from a continuous layer of GB $\alpha$ , a mixture of GB $\alpha$  with WS emanating from it, to WS alone developing directly from bare  $\beta$  GB. The critical angles at which the morphology changes from

one to another can also be determined based on the simulation results.

Specimen of Ti-5Al-5Mo-5V-3Cr (wt.%) was  $\beta$ -solutionized at 1000 °C for 30 min and water-quenched to room temperature, subsequently, up-quenched to 700 °C and isothermally held for 2 hrs, followed by water quenching. The microstructures were characterized by SEM backscattered electron (BSE) imaging and electron backscattered diffraction (EBSD) in a ThermoScientific Scios 2 FIB/SEM equipped with EDAX Hikari EBSD Camera. 3D morphology of the  $\alpha$  precipitates were obtained by FIB serial sectioning and reconstructed using the MIPAR image analysis software [21] (see Supplementary materials S.1.for greater details).

The BSE (Fig. 1(a)) and the corresponding EBSD OIM (Fig. 1(b)) images show both grain boundary and intragranular areas. Three prior  $\beta$  grains are decorated by GB $\alpha$  and  $\alpha$  side plates at or near  $\beta$  GBs as well as intragranular  $\alpha$  precipiates within grain interior. The three  $\beta$  grains are further reconstructed from the  $\alpha$ -phase orientation map in Fig. 1(b) (see

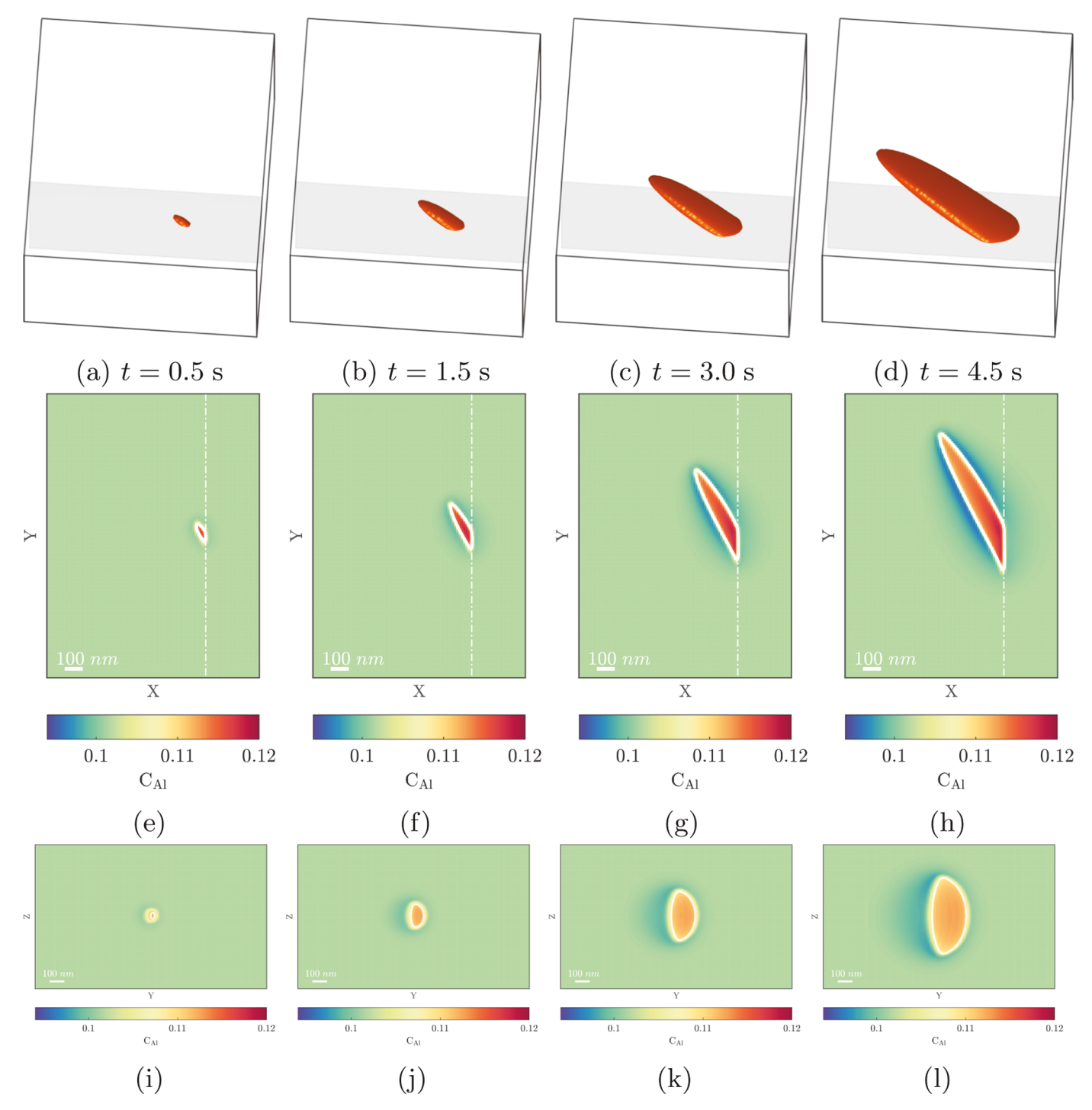


**Fig. 2.** Morphological evolution of a single  $\alpha$  precipitate at a  $\beta$  grain boundary. The inclination angle  $\theta$  between the grain boundary plane (as indicated by the light gray plane in the first row and the white dashed line in the second row) and the habit plane of the  $\alpha$  precipitate is 30°. The white solid contour line denotes the  $\alpha$  / $\beta$  interface at which the phase field order parameter  $\phi = 0.5$ .

Fig. 1(c) for the IPF) and are referred to as  $\beta_1$ ,  $\beta_2$ ,  $\beta_3$ , respectively. Fig. 1 (d) shows 3D images of the  $\alpha$  precipitates formed at and near GBs as highlighted by the dashed square. A significant morphological variation for precipitates at and near GBs can be clearly observed: At  $\beta_1$  / $\beta_3$  GB,  $\alpha$  precipitates of a single orientation variant (referred to as GB $\alpha_2$ ) appear as a continuous layer alone without forming colony WS; at  $\beta_2$  / $\beta_3$  GB,  $\alpha$  precipitates (of another single variant and is referred to as GB $\alpha_1$ ) look like a mixture of a continuous layer of GB $\alpha$  and WS emanating from it; at  $\beta_1/\beta_2$  GB,  $\alpha$  precipitates, consisting of multiple variants, appear as discrete particles. Orientation analysis (see supplementary materials S2

for details) shows that  $GB\alpha_1$  maintains Burgers orientation relationship (BOR) with the  $\beta_3$  (Supplementary Table 1 and Fig. 1). Thus, WS colony, which appear to stem from Mullis-Sekerka interface instability [22] operating at the surface of  $GB\alpha_1$ , grow into the Burgers grain  $\beta_3$  [12]. The physical contact between  $GB\alpha$  and the WS (colony) is confirmed by the 3D reconstruction shown in (Figs. 1(e)-(e'')). 3D morphology of  $GB\alpha_2$  (Figs. 1(f)-(f'')) shows that it is indeed a continuous layer spreading over the whole GBP without branching out [17]. From Fig. 1 (b),  $GB\alpha_2$  is found to have the same color as one type of discrete precipitates (referred to as  $GB\alpha_3$ ). Further orientation analysis

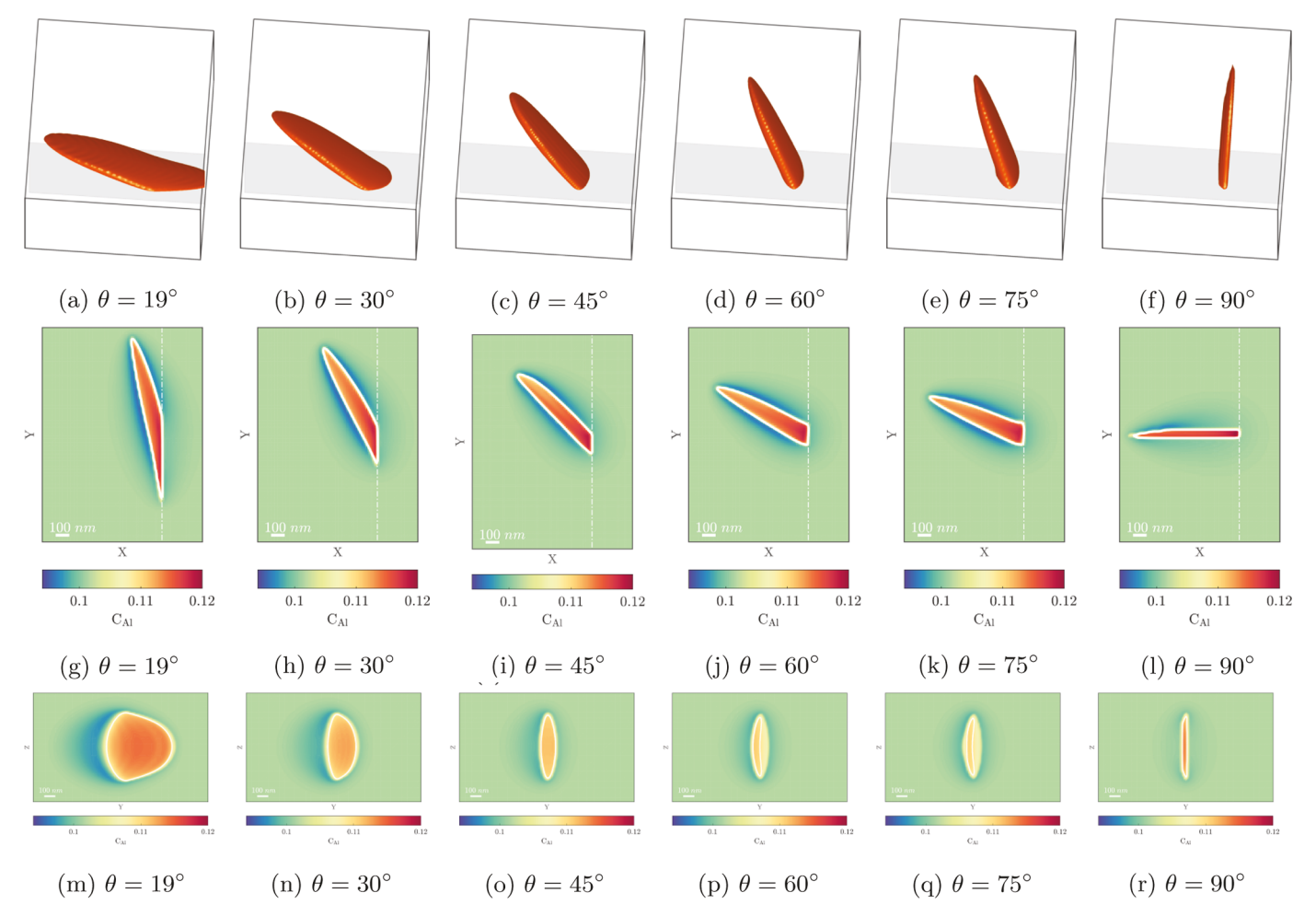


**Fig. 3.** Morphology of a single  $\alpha$  precipitate at a  $\beta$  GB (at t=5.0 s) as a function of  $\theta$ .

(Supplementary Tables 2-3 and Supplementary Figs. 2-3) indicates that they both keep BOR with  $\beta_1$  and belong to the same orientation variant. 3D morphology of  $GB\alpha_3$  is shown in (Figs. 1(g)-(gg'')).

Analysis of VS behaviors for these three GB precipitates indicates that GBP inclination determines the VS of GB $\alpha$  for all these three cases instead of GB misorientation. First, none of the selected variant has the smallest deviation from BOR, which is quantified by the disorientation angle  $\theta_m$  associated with the deviation matrix ( $\beta \Delta J \beta^{\rm BOR}$ ), and all 24 possible  $\theta_m$  are larger than 15° (see supplementary materials S2) [10, 12]. Here ( $\beta \Delta J \beta^{\rm BOR}$ ) is a quantitative measure of the deviation of the OR between the GB $\alpha$  and the non-Burgers grain from the BOR [12]. Second, the inclination angles  $\theta$  are somewhat randomly scattered, which are 73.18, 0 and 90° for GB $\alpha_1$ , GB $\alpha_2$  and GB $\alpha_3$ , respectively. Thus, only the VS for the GB $\alpha_2$  may have followed the empirical rule (i. e., HP should be parallel to GBP).

To elucidate the physics underlying the morphological variation of  $\alpha$  precipitates at GBs, a three-dimensional phase field model for an elastically and structurally inhomogeneous system is employed to simulate the nucleation and growth of  $\alpha$  precipitate at the  $\beta$  GB in a bicrystalline  $\beta$  Ti-6Al-4V (wt.%, Ti64) as a function of  $\theta$ . The model builds upon our previous work on the effect of GB dislocation network, applied stress/strain and cooling rates on  $\alpha$  precipitation in a polycrystalline  $\beta$  sample [23,24,25] (see supplementary materials S3). The  $\beta$  bicrystal is constructed by first halving the perfect crystal along the  $(010)_{\beta}$  plane and rotating the two resulting grains by  $\eta_2$  for  $\beta_2$  on left-hand side and  $\eta_1$  for  $\beta_1$  on right-hand side, respectively, around the  $[101]_{\beta}$  direction.

We started by investigating the influence of  $\theta$  on the morphology development of a single  $\alpha$  precipitate during its growth at a GB. The

growth is initiated by an over critical  $\alpha$  phase nucleus placed in the middle of the GBP and takes an initial shape of a spherical cap. The variant selected for GB $\alpha$  maintains BOR with  $\beta_2$  as described by  $(101)_{\beta}\|(0001)_{\alpha}$ ,  $[\overline{1}11]_{\beta}\|[11\overline{2}0]_{\alpha}$  (Eq. (1)). A  $\theta=30^{\circ}$  between HP of the selected  $\alpha$  precipitate and the GBP is achieved by selecting  $\eta_1=-2.0\times5.26^{\circ}$  and  $\eta_2=3.7\times5.26^{\circ}$  (see Supplementary Table 4).

The morphological development during growth is demonstrated in Fig. 2, with Figs. 2(a)-(d) at the top showing the microstructure evolution of the  $\alpha$  precipitate in 3D, and Figs. 2(e)-(h) in the middle showing the corresponding 2D Al concentration mapping normal to the GBP through the center of the simulation box, and Figs. 2(i)-(l) at the bottom showing the corresponding 2D concentration mapping on the GBP at different time within t = 0.5 - 4.5 s. As can be observed from 2D crosssections both normal to and along the GBP (represented by a light gray plane), upon growth, the overcritical  $\alpha$  precipitate not only spreads along the GBP but also grows into the  $\beta_2$  grain interior. The lateral growth leads to the formation of the typical  $GB\alpha$  structure (Fig. 2(1)). Besides that, the  $\alpha$  precipitate develops into a lath with a well-defined HP, emanating from the GB $\alpha$  and growing into  $\beta_2$  grain interior as a typical WS structure (Fig. 2(h)). As a result, at t = 4.5 s, the  $\alpha$  precipitate appears as a mixture of  $GB\alpha$  and WS emanating from it (Fig. 2(d)). An accompanying depletion layer of  $\alpha$  stabilizers (e.g., Al) has developed in the surrounding  $\beta$  matrix. The simulation results suggest that morphological development and the resulting morphology are determined by the dynamic interplay between lateral growth (i.e., spreading) along the GBP and the development of the  $\alpha$  side plate emanating from the GB $\alpha$ , both of which are sensitive to  $\theta$  as shown below.

Fig. 3 maps the morphology of a single  $\alpha$  precipitate at a GB (at t=

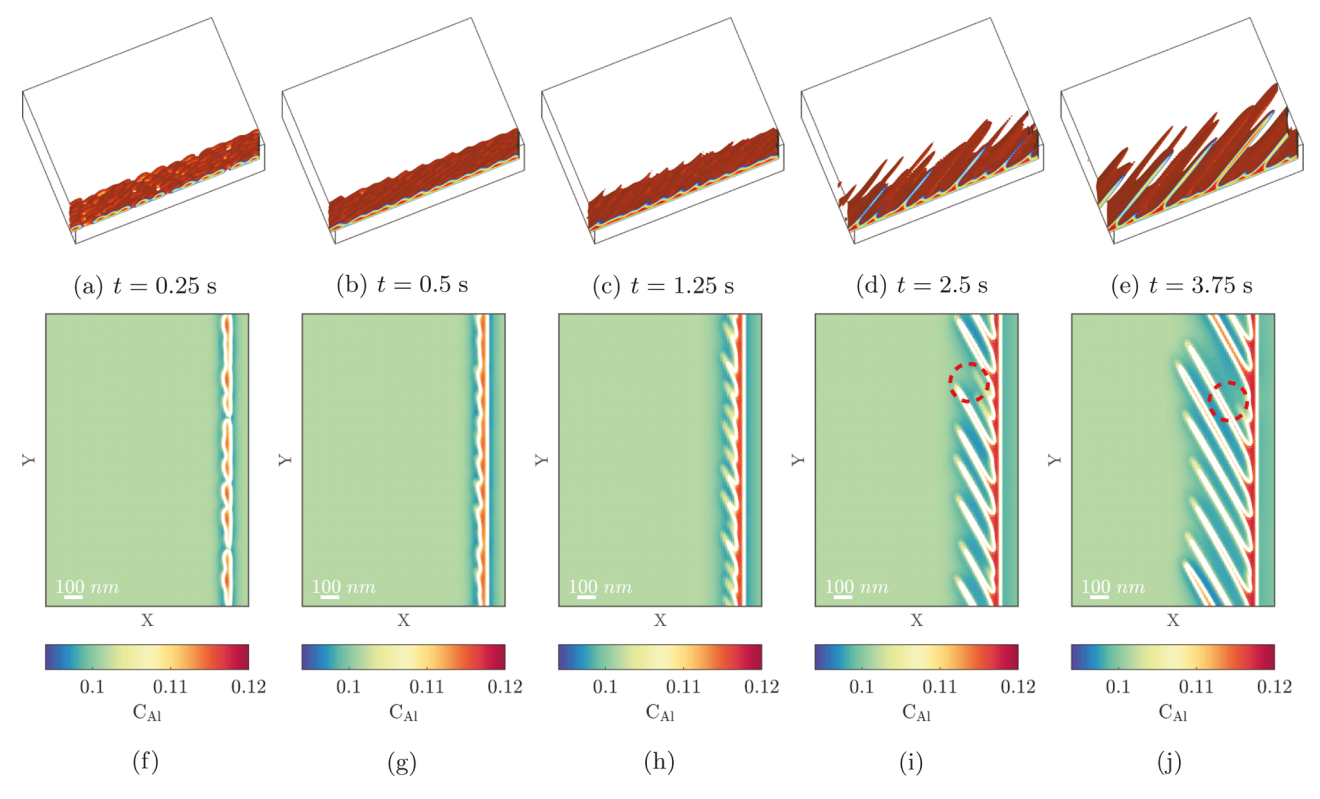


**Fig. 4.** Morphological evolution of  $\alpha$  precipitates nucleated at a  $\beta$  grain boundary. The inclination angle  $\theta$  between the grain boundary plane and the habit plane of the  $\alpha$  precipitate is 30°.

5.0 s) as a function of  $\theta$ . Apparently, the area of GB $\alpha$  layer projected on the GBP (i.e., the extent of lateral growth on the GBP, Figs. 3(m)-(i),) decreases while the length of the  $\alpha$  lath into grain interior increases with increasing  $\theta$  (i.e., the area of the broad face developed into grain interior increases, Figs. 3(g)-(l)), respectively. In other words, WS gains growth advantage over the lateral spreading of GB $\alpha$  along a GB with increasing  $\theta$ . Consequently, with increasing  $\theta$ , there is a gradual morphological

transition from a mixture of GB $\alpha$  layer and WS, to a WS alone that appears as directly emanating from the bare GBP (see e.g., at  $\theta = 90^{\circ}$  (Figs. 3(l, f, r)).

We now consider concurrent nucleation and growth of multiple  $\alpha$  precipitates at a GB during isothermal aging. To do so, the so-called explicit nucleation algorithm is implemented and integrated with the phase-field model. The algorithm stochastically seeds nuclei in an

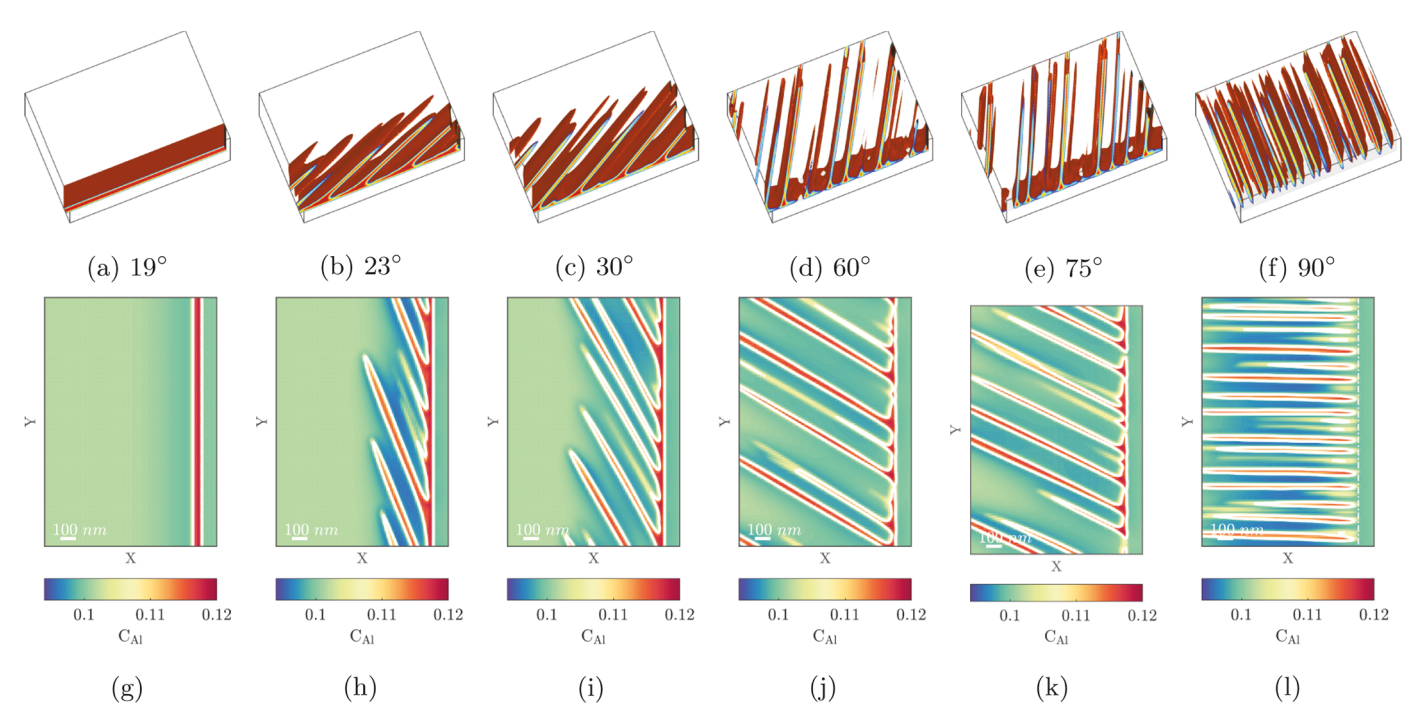


**Fig. 5.** Morphology of  $\alpha$  precipitate nucleated at a  $\beta$  GB (at t=5.0 s) as a function of  $\theta$ .

R. Shi et al. Scripta Materialia 214 (2022) 114651

evolving microstructure according to the nucleation rates calculated as a function of local concentration, temperature and crystalline defects (i.e., GBs) [24,26]. For simplicity, we consider that all GB precipitates maintain BOR with  $\beta_2$  and belong to a single variant as described by Eq. (1). We started again from considering  $\theta = 30^{\circ}$  (Fig. 4). Individual  $\alpha$ precipitates first nucleate and grow independently until all the available nucleation sites are occupied. A total number of 36  $\alpha$  precipitates nucleate heterogeneously at the GBP. These discrete  $\alpha$  precipitates first grow independently and then coalescence (among the same variant) with each other, forming an extended layer of  $GB\alpha$  completely covering the GB. Also noticed is that protrusions on the surface (Figs. 4(b) and (g)) of the continuous  $\alpha$  films gradually develop into  $\alpha$  laths with well-defined habit plane (Figs. 4(d) and (i)). Overtime, the progressive growth of  $\alpha$  laths towards grain interior leads to the formation of a microstructure that is dominated by  $\alpha$  colonies of parallel laths emanating as side plates from the nearly continuous grain boundary  $\alpha$ film (Figs. 4(e) and (j)). During the growth into grain interior, coarsening among WSs takes place and the longer WS further grow at the expense of the relatively small ones (encircled by the red dashed lines, Figs. 4(i) and (j)).

Fig. 5 maps the morphology of GB precipitates as a function of  $\theta$ . Three distinct regimes of GB precipitate morphology are readily observed, which can be separated by two critical angles  $\theta_c^1$  and  $\theta_c^2$ :  $\theta < \theta_c^1$ , GB $\alpha$  alone appears as a continuous layer covering the whole GB (see Fig. 5(a) for  $\theta=19^{\circ}$ ),  $\theta_c^1<\theta\leq\theta_c^2$ , the morphology of  $\alpha$  precipitate looks like a mixture of  $GB\alpha$  layer and WS emanating from it (Figs. 5(b)-(e));  $\theta > \theta_c^2$ , WS alone grows directly from the bare  $\beta$  GB without forming GB $\alpha$  (Figs. 5(f) and (l)). Note that in regime II, the morphology of GB $\alpha$  evolves from a continuous layer (Fig. 5(h)) into discrete particles (Fig. 5(k)), while the number (as can be seen from the areal number density of side plates) and the length of WS into grain interior increase with increasing  $\theta$ . The transition in the morphology suggests that WS gradually gains growth advantage over the lateral growth of  $GB\alpha$ . Even the number of simulations in the current study is not enough to resolve these two critical angles, the observed morphological transition suggests that  $19^{\circ} < \theta_c^1 < 23^{\circ}$  and  $75^{\circ} < \theta_c^2 < 90^{\circ}$ .

The simulation results above make clear that the morphological variation of  $\alpha$  precipitates at a  $\beta$  GB originates from the inclination angle  $\theta$  dependence of the dynamic interplay between the spreading over the GBP and the growth into grain interior as a WS during precipitate growth. Even though both processes are driven by the chemical free energy reduction, the former and the thus formation of  $GB\alpha$  is promoted by the area reduction of the pre-existing GB, while the latter is energetically favorable by the  $\alpha/\beta$  interfacial energy and strain energy minimization through developing an optimum shape having a broad face with its orientation corresponding to the direction at which the elastic strain energy density is minimized [27]. Depending on the magnitude of  $\theta$ , two processes could be competing against or complementary to each other. For example, at  $\theta=0^{\circ}$ , there exists a pronounced tendency for the HP developed to be parallel to the GBP. Doing so not only maximizes the area of GB eliminated by the GB $\alpha$  but also minimizes the elastic strain energy. Consequently, spreading of multiple  $\alpha$  precipitates of the same orientation variant and the subsequent coalescence leads to the formation of a continuous layer of  $GB\alpha$  without the presence of WS. Following the fact that an optimum shape with a well-defined habit plane (or broad face) orientation offers a relative low interface energy as well as low elastic strain energy for a precipitate with a given volume, any deviation from it (measured by  $\theta$ ), will result in a rise in the value of these energy terms. Therefore, as  $\theta$  increases, the lateral growth or spreading over the GBP will be gradually suppressed because the concomitant development of a "wrong" habit plane (i.e., GBP) would result in a significant increase in both strain energy and interface energy

Consequently, WS develops during continued increase of  $\theta$  when the elastic strain energy and interfacial energy contribution to the total free

energy of the system become dominant. Formation of WS relieves the elastic strain energy built up due to developing a non-optimum habit plane at the expense of increasing both interface and elastic strain energy. Consequently, precipitate morphology transits from a continuous GB $\alpha$  layer to a mixture of GB $\alpha$  and WS emanating from it, and eventually, a pure WS without forming GB $\alpha$  (see, e.g.,  $\theta=90^\circ$ ). Morphologies of three GB precipitates observed in the present experiments support the above analysis (Fig. 1), for which the  $\theta$  are 73.18, 0 and 90° for GB $\alpha_1$  to GB $\alpha_3$ , respectively.

Several assumptions made in the current study need to be noted. First of all, nucleation and growth of multiple  $\alpha$  precipitates of the same orientation variant at a  $\beta$  GB are considered in the present study. However, it is frequently observed that multiple  $\alpha$  precipitates of different orientation variants form simultaneously at the same GB. As a result, they impinge upon each other during spreading along the same GBP and form more or less equiaxed GB $\alpha$  (instead of a continuous  $\alpha$  film) due to the spatial confinement from neighboring variants of dissimilar type. Moreover, when developing into grain interior as a side plate, spatial confinement or hard impingement between side plates of different variants may also occur since their habit planes have different inclination angles relative to the same GBP. This may explain the experimentally observed diverse morphology of grain boundary precipitates. It should be emphasized that such interactions do not change the nature of dynamic interplay between two key processes, i.e., the spreading along GBP and the intragranular growth of the GB precipitate, during the growth of GB precipitate of arbitrary variant. Secondly, instead of developing a phase-field model for the experimental model system Ti-5553, we employed the phase-field model developed for Ti-6Al-4V system to elucidate the underlying mechanism(s) for the morphological variation. However, this discrepancy in alloy composition will not qualitatively change the result. This is because two key processes as revealed by the current simulations are universal in whatever alloy systems as long as nucleation of precipitates occur at GBs.

In summary, the results represent an important progress towards understanding the formation mechanisms for key microstructure features of second-phase precipitate that have profound influence on mechanical properties in Ti-alloys. Moreover, the advantage of using advanced 3D computational and characterization tools in a correlative manner for understanding complex microstructure development are applicable to a wide range of metallic materials beyond Ti alloys.

#### **Declaration of Competing Interest**

The authors declare that they have no known competing financial interests or personal relationships that could have appeared to influence the work reported in this paper.

### Acknowledgement

This work has been supported by the open research fund of Songshan Lake Materials Laboratory (2021SLABFK06) and start-up funding from Harbin Institute of Technology (Shenzhen). DL and YZ appreciate the financial support from University of Nevada Reno Research Enhancement Grants and National Science Foundation, grant CMMI-2122272.

### Supplementary materials

Supplementary material associated with this article can be found, in the online version, at doi:10.1016/j.scriptamat.2022.114651.

#### References

- [1] D. Banerjee, J.C. Williams, Acta Mater. 61 (3) (2013) 844–879.
- [2] M.R. Bache, Int J Fatigue 21 (1999) S105-S111.
- [3] R. Shi, Y. Gao, D. Li, W. Zhao, Y. Zheng, Adv. Eng. Mater. 23 (8) (2021), 2100152.
- [4] G. Lütjering, Mater. Sci. Eng. 243 (1) (1998) 32-45.

- [5] S.M.C. van Bohemen, A. Kamp, R.H. Petrov, L.A.I. Kestens, J. Sietsma, Acta Mater. 56 (20) (2008) 5907–5914.
- [6] M. Salib, J. Teixeira, L. Germain, E. Lamielle, N. Gey, E. Aeby-Gautier, Acta Mater. 61 (10) (2013) 3758–3768.
- [7] T. Ahmed, H.J. Rack, Mat. Sci. Eng. A Struct 243 (1-2) (1998) 206-211.
- [8] D. Bhattacharyya, G.B. Viswanathan, R. Denkenberger, D. Furrer, H.L. Fraser, Acta Mater. 51 (16) (2003) 4679–4691.
- [9] E. Lee, R. Banerjee, S. Kar, D. Bhattacharyya, H.L. Fraser, Philos. Mag. 87 (24) (2007) 3615–3627.
- [10] R. Shi, V. Dixit, G. Viswanathan, H. Fraser, Y. Wang, Acta Mater. 102 (2016) 197–211.
- [11] M. Salib, J. Teixeira, L. Germain, E. Lamielle, N. Gey, E. Aeby-Gautier, Acta Mater. 61 (10) (2013) 3758–3768.
- [12] R. Shi, V. Dixit, H.L. Fraser, Y. Wang, Acta Mater. 75 (0) (2014) 156-166.
- [13] N. Stanford, P.S. Bate, Acta Mater. 52 (17) (2004) 5215-5224.
- [14] S.C. Wang, M. Aindow, M.J. Starink, Acta Mater. 51 (9) (2003) 2485-2503.
- [15] T. Furuhara, S. Takagi, H. Watanabe, T. Maki, Metall. Mater. Trans. A 27 (6) (1996) 1635–1646.

- [16] T. Furuhara, T. Maki, Mater. Sci. Eng. 312 (1) (2001) 145-154.
- [17] H. Sharma, S.M.C. van Bohemen, R.H. Petrov, J. Sietsma, Acta Mater. 58 (7) (2010) 2399–2407.
- [18] R. Shi, D. Choudhuri, A. Kashiwar, S. Dasari, Y. Wang, R. Banerjee, D. Banerjee, Philos. Mag. (2021) 1–24.
- [19] S. Balachandran, A. Kashiwar, A. Choudhury, D. Banerjee, R. Shi, Y. Wang, Acta Mater. 106 (2016) 374–387.
- [20] M.V. Kral, G. Spanos, Metall. Mater. Trans. A 36 (5) (2005) 1199–1207.
- [21] J.M. Sosa, D.E. Huber, B. Welk, H.L. Fraser, Integrat. Mater. Manuf. Innov. 3 (1) (2014) 123–140.
- [22] W.W. Mullins, R.F. Sekerka, J. Appl. Phys. 34 (2) (1963) 323-329.
- [23] R. Shi, N. Zhou, S. Niezgoda, Y. Wang, Acta Mater. 94 (2015) 224-243.
- [24] R. Shi, S. Khairallah, T.W. Heo, M. Rolchigo, J.T. McKeown, M.J. Matthews, JOM 71 (10) (2019) 3640–3655.
- [25] D. Qiu, R. Shi, P. Zhao, D. Zhang, W. Lu, Y. Wang, Acta Mater. 112 (2016) 347–360.
- [26] J.P. Simmons, C. Shen, Y. Wang, Scr. Mater. 43 (10) (2000) 935-942.
- [27] R. Shi, N. Ma, Y. Wang, Acta Mater. 60 (10) (2012) 4172-4184.